The Extratropical Tropopause Inversion Layer: Global Observations with GPS Data, and a Radiative Forcing Mechanism

WILLIAM J. RANDEL AND FEI WU

National Center for Atmospheric Research, Boulder, Colorado*

PIERS FORSTER

School of Earth and Environment, University of Leeds, Leeds, United Kingdom

(Manuscript received 25 January 2007, in final form 2 March 2007)

ABSTRACT

Global characteristics of the extratropical tropopause inversion layer identified in radiosonde observations by Birner are studied using high vertical resolution temperature profiles from GPS radio occultation measurements. The GPS data are organized according to the height of the thermal tropopause in each profile, and a temperature inversion layer above the tropopause (with an average magnitude of 3–5 K) is found to be a ubiquitous, climatological feature. The GPS data show that the inversion layer is present for all seasons in both hemispheres, spanning the subtropics to the pole, and there is not strong longitudinal structure. Dependence of the inversion layer on upper-troposphere vorticity is studied; while anticyclones exhibit a substantially stronger inversion than cyclones (as expected from balanced dynamics), the inversion is evident for all circulation types. Radiative transfer calculations indicate that strong gradients in both ozone and water vapor near the tropopause contribute to the inversion. Significant absorption of both longwave and shortwave radiation by ozone occurs, warming the region above the tropopause. Water vapor near and immediately above the tropopause contributes to cooling, effectively enhancing the inversion.

1. Introduction

Several recent observational studies have used high vertical resolution radiosonde measurements to document a persistent inversion layer above the extratropical tropopause (Birner et al. 2002; Birner 2006). These analyses were based on radiosonde data from two German stations (Birner et al. 2002), and from 80 U.S. stations spanning the Tropics to polar regions (Birner 2006). The results of these studies showed that when radiosonde profiles are averaged using a tropopause-based coordinate system, the mean structure exhibits a clear inversion in a relatively narrow layer above the tropopause (and a corresponding layer of enhanced static stability). This inversion structure is smeared out and not evident for averages calculated in geometric height. Birner (2006) furthermore showed that the tropopause inversion layer (TIL) is evident in radiosonde wind measurements, reflecting thermal wind balance with the temperature structure.

The TIL is a relatively new observational feature, and as yet no simple explanation is available. Wirth (2003) has shown that enhanced stability above the tropopause is a feature of anticyclonic upper-tropospheric flow expected from large-scale balanced dynamics; in contrast, cyclonic circulation does not exhibit this behavior. His analysis suggested that the TIL could be evident in time-averaged statistics as a result of this anticyclonic influence. This analysis has been extended by Wirth (2004) and Wirth and Szabo (2007) to quantify the dynamical mechanisms leading to tropopause sharpening (which occurs primarily in anticyclonic flow). Birner (2006) suggested that the TIL could result from large-scale poleward heat fluxes (associated with deep extratropical baroclinic eddies), acting on the background temperature gradient in the tropopause region. We discuss these ideas in light of the GPS observations below.

* The National Center for Atmospheric Research is sponsored by the National Science Foundation.

Corresponding author address: William J. Randel, NCAR, P.O. Box 3000, Boulder, CO 80307.
E-mail: randel@ucar.edu

DOI: 10.1175/2007JAS2412.1

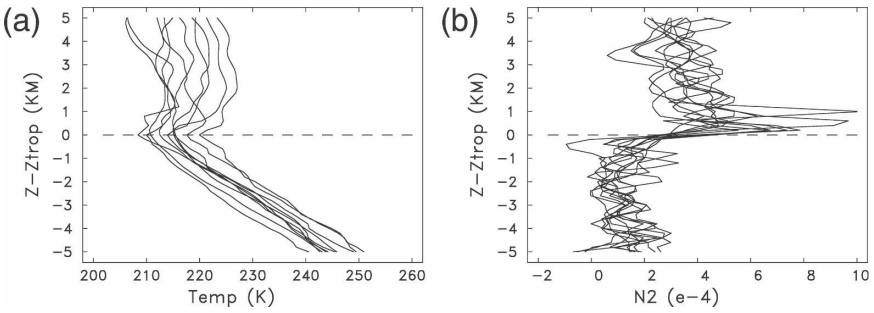

FIG. 1. Vertical profiles of (left) temperature and (right) static stability N^2 derived from GPS measurements over 40°–50°N on 9 Jan 2004. The vertical coordinate is calculated with respect to the thermal tropopause in each profile.

One objective of this paper is to characterize the global behavior of the TIL, based on GPS radio occultation temperature data. These data have high vertical resolution, with the ability to observe the TIL on a global scale. We use a coordinate system based on the lapse rate tropopause for each profile, and quantify the structure of the TIL, together with its latitudinal, seasonal, and hemispheric characteristics. We also study the relationship of TIL structure to upper-tropospheric circulation (relative vorticity at 200 hPa) based on National Centers for Environmental Prediction (NCEP) reanalysis meteorological data collocated with the GPS temperature profiles, in order to quantify dynamical influence on the inversion layer. Finally, we investigate the contribution of radiative heating to formation and maintenance of the inversion layer, based on detailed radiative transfer calculations including observed ozone and water vapor profiles organized in tropopause-based coordinates.

2. Data and analyses

The high vertical resolution and high accuracy of GPS radio occultation temperature measurements were demonstrated by the GPS/MET satellite (Kursinski et al. 1996; Rocken et al. 1997). In this work we use GPS temperature data from the Challenging Minisatellite Payload (CHAMP; Wickert et al. 2001), including data spanning the years 2001–06. Hajj et al. (2004) have extensively characterized and compared the CHAMP temperature retrievals and demonstrate that individual profiles are precise to <0.6 K over 5–15 km, increasing slightly to ~2 K at 25 km. The vertical resolution of GPS retrievals can approach ~100 m, but the data used here are sampled on a 200-m grid. We focus on the altitude range around the extratropical tropopause, spanning approximately 5–15 km, covering latitudes poleward of 20° in both hemispheres. For each hemisphere, the 5 yr of data analyzed here provide about 23 000 profiles for each 3-month season.

Following Birner et al. (2002) and Birner (2006) we use a vertical coordinate system based on the first lapse rate tropopause [Z_{LRT1}, using the standard World Meteorological Organization (WMO) lapse rate criterion]. For each GPS temperature profile, we calculate Z_{LRT1} and then calculate vertical structure with respect to this level. We exclude profiles where $Z_{\mathrm{LRT1}} > 14$ km, which are characteristic of the tropical tropopause. Figure 1 shows an example of 10 GPS temperature profiles covering 40°–50°N on 9 January 2004, organized in a coordinate system relative to Z_{LRT1} (Z_{LRT1} spanned a range of ~9–12 km for these cases; hereafter Z_{LRT1} is referred to as the tropopause). Most of the temperature profiles in Fig. 1a exhibit a temperature increase above the tropopause, and this corresponds to the TIL, which is the focus here (as shown below, the overall warmer profiles in Fig. 1a are associated with cyclonic circulation systems, which have a lower Z_{LRT1} and systematically higher temperatures). Figure 1b shows the corresponding Brunt–Väisälä frequency squared (N^2) for these temperature profiles, which is a useful measure of the stability characteristics (Andrews et al. 1987). The profiles in Fig. 1b show a relative maximum in N^2 within 1 km above the tropopause, with somewhat smaller values at higher altitudes (and much smaller values in the troposphere). We focus on the statistical behavior of temperature and N^2 derived from the GPS profiles in the tropopause coordinate system, in order to characterize global characteristics of the TIL.

3. GPS observations

a. Cyclones, anticyclones, and TIL structure

Wirth (2003) studied the balanced dynamics of tropopause potential vorticity anomalies and demonstrated that enhanced stability in the TIL is a characteristic of

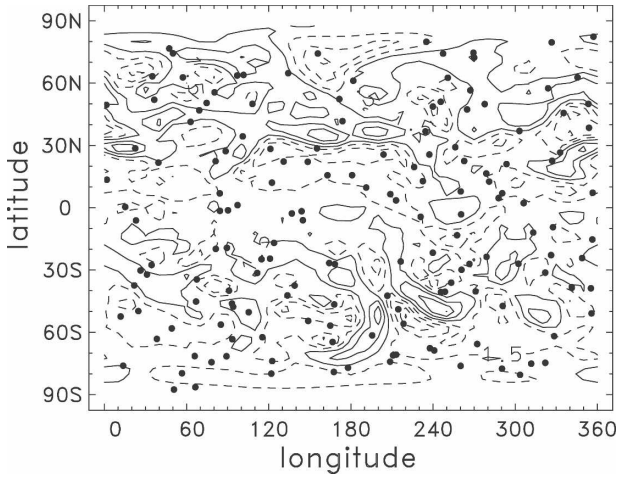

FIG. 2. Contours show relative vorticity at 200 hPa on 9 Jan 2004, calculated from NCEP reanalysis data; contours are ± 1.5, 4.5, ... $\times 10^{-4}$ s^{-1}. The dots indicate locations of CHAMP GPS temperature soundings for this day.

extratropical anticyclones; cyclonic circulation systems did not exhibit a TIL in these calculations. These results suggested that the climatological structure observed by Birner et al. (2002) could result from averaging across a range of circulation systems. To explore the relationship between tropopause structure and large-scale circulation, we use relative vorticity (ζ) on the 200-hPa level derived from the NCEP reanalysis (Kalnay et al. 1996) to classify the near-tropopause circulation. Relative vorticity is calculated on a daily basis, and sampled at each of the GPS temperature profile locations; an example of the spatial sampling for one day is shown in Fig. 2. The GPS profiles are then binned according to the relative vorticity fields, in order to separate cyclonic (positive ζ) versus anticyclonic (negative ζ) structure. Figure 3a shows the distribution of 200-hPa relative vorticity over 30°–60°N during December–February (DJF) from this sampling, showing a skew in the distribution toward cyclonic vorticity (this is characteristic of both NH and SH statistics). Figure 3b shows the mean height of the tropopause within each vorticity bin, revealing a monotonic shift from relatively high tropopause (~12 km) for anticyclones to a lower tropopause (~10 km) for cyclonic circulation. This behavior is expected based on balanced dynamical structure (e.g., Hoskins et al. 1985; Zangl and Wirth 2002). The detailed structure in Fig. 3b shows a relatively constant tropopause height for strongly cyclonic circulations ($\zeta > 2 \times 10^{-4}$ s^{-1}). This behavior is probably related to the separation of the thermal and dynamical tropopauses in strongly cyclonic circulation systems (Wirth 2000, 2001). This is confirmed by an analogous calculation of the height of the dynamical tropopause (based

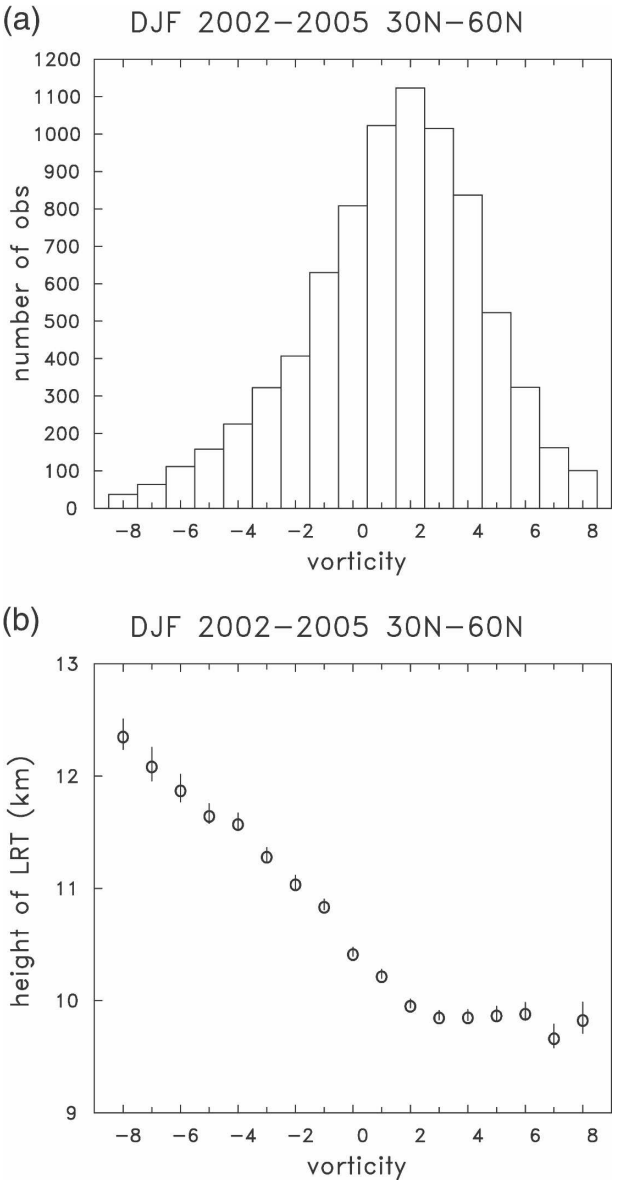

FIG. 3. (a) Distribution of relative vorticity (10^{-4} s^{-1}) at 200 hPa over 30°–60°N during DJF, sampled at the GPS observation locations during 2001–06. (b) Altitude of Z_{LRT1} derived from the GPS temperature profiles averaged within each vorticity bin. The circles show the mean values, and the error bars denote the std dev of the means.

on potential vorticity), which reveals a more continuous altitude change over the entire range of vorticity (results not shown here).

Figure 4 compares the temperature and N^2 structure for GPS profiles composited from cyclonic vorticity ($\zeta > 3 \times 10^{-4}$ s^{-1}), near-zero vorticity ($-2 < \zeta < 2$), and anticyclonic vorticity ($\zeta < -3$), for NH DJF statistics over 30°–60°. The temperature profiles for each group (Fig. 4a) show a clear inversion, with tempera-

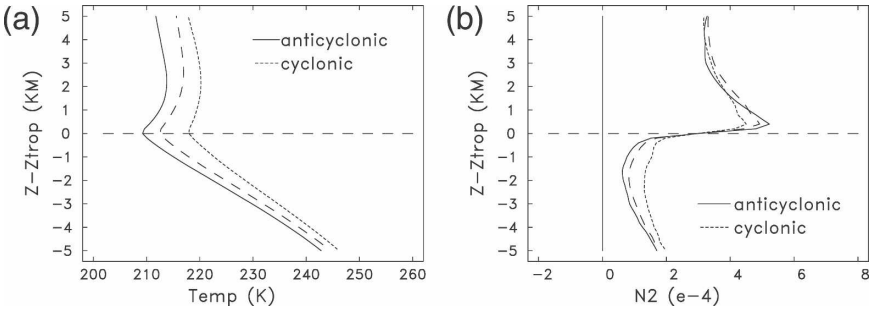

FIG. 4. (a) Vertical profile of GPS temperature in tropopause-based coordinates, sampled over 30°–60°N during DJF, separated according to the relative vorticity (ζ) near the profile at 200 hPa. Results are separated for strongly cyclonic ($\zeta > 3 \times 10^{-4}$ s^{-1}), near-zero ($-2 < \zeta < 2$), and anticyclonic ($\zeta < -3$) circulation systems (as shown in Fig. 3). (b) Corresponding profiles of static stability parameter N^2.

ture increases of ~3–5 K above the tropopause. The tropopause inversion is somewhat stronger for anticyclonic flow, but is present in all cases. This is shown more explicitly in Fig. 5, where the average strength of the inversion (defined by the temperature difference between $Z_{\mathrm{LRT1+2\,km}}$ and Z_{LRT1}) is calculated within each vorticity bin. This shows that the inversion strength varies more or less monotonically with vorticity, ranging from ~1 K for strongly cyclonic flow to ~6 K for strongly anticyclonic circulation; the inversion is approximately 4 K for near-zero vorticity. The height of the maximum temperature is 2–3 km above the tropopause, and is not strongly dependent on vorticity (not shown).

The N^2 structures for the vorticity bins in Fig. 4b show a clear maximum above the tropopause in each case, with the highest stability for anticyclonic vorticity cases. The maximum N^2 occurs within 1 km above the tropopause, and varies from approximately 4.5 (cyclonic) to 5.5×10^{-4} s^{-2} (anticyclonic flow). The GPS results in Fig. 4 are similar to the radiosonde-based statistics in Birner (2006), although the radiosonde results show a somewhat larger maximum in N^2 (above 6.0×10^{-4} s^{-2}) with a peak nearly coincident with the tropopause. This sharper structure may be due to the higher vertical resolution of the radiosondes (30 m) compared to GPS (200 m). There are also substantial differences in tropospheric stability in Fig. 4b, with anticyclonic circulation having very low stability below the tropopause (this is also characteristic of balanced dynamical structure; e.g., Hoskins et al. 1985). We note that a result similar to Fig. 4 was derived by Birner (2006), based on sampling statistics according to the height of Z_{LRT1} rather than near-tropopause relative vorticity (although these are closely related, as shown in Fig. 3b). Results similar to Figs. 4 and 5 are seen for GPS temperature profiles in both hemispheres and for all seasons (not shown here). The key point is that, while the enhanced stability layer above the tropopause (the TIL) is strongest for anticyclonic circulation, it is also apparent for cases with near-zero vorticity, and even for strongly cyclonic situations. Hence, the enhanced stability layer is a general property of the extratropical tropopause for all dynamical situations.

b. Global TIL structure

The near-global structure of the extratropical TIL based on GPS data is shown in Fig. 6. Here the N^2 structure in tropopause coordinates is calculated for 10° latitude bands spanning 20°–90° in each hemisphere

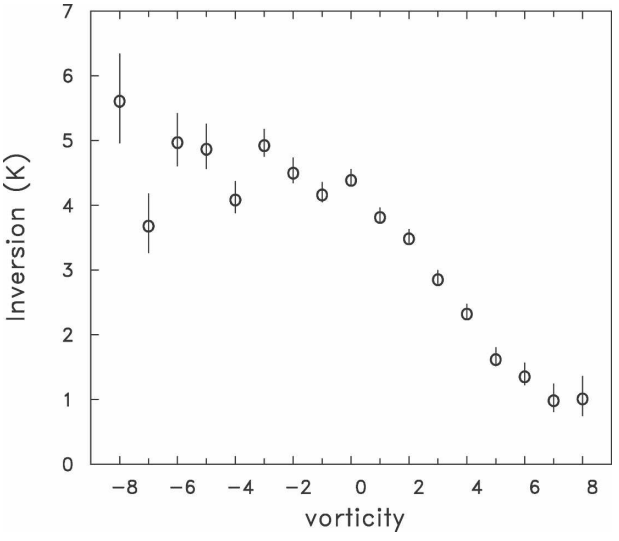

FIG. 5. Strength of the tropopause inversion as a function of relative vorticity, quantified as the temperature difference between $T_{\mathrm{ZLRT+2\,km}}$ minus T_{ZLRT}. The circles show the mean within each vorticity bin (with sampling as in Fig. 3), and the error bars denote the standard deviation of the means.

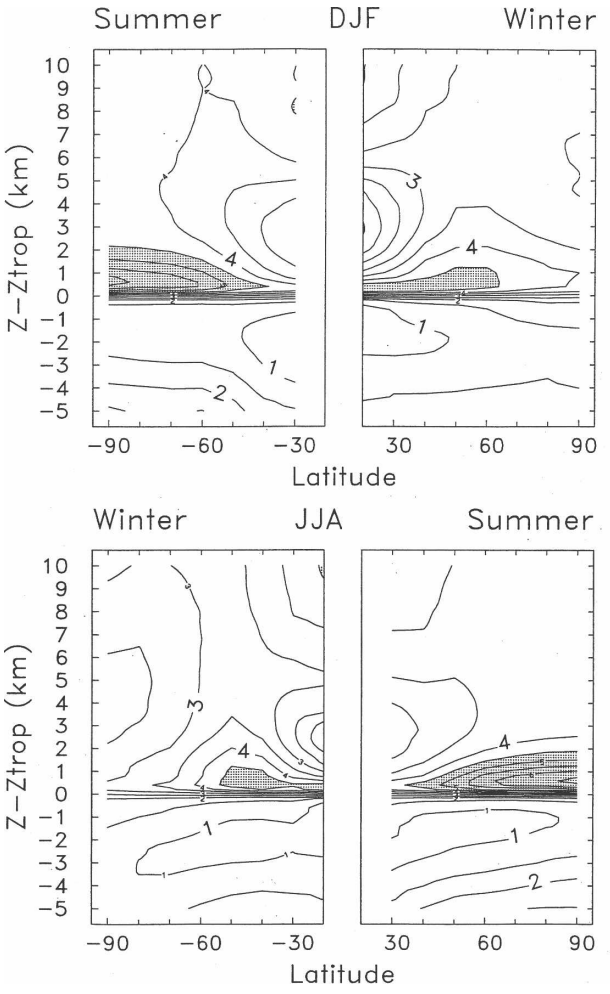

FIG. 6. Latitude–height cross sections of climatological N^2, derived from GPS data organized in tropopause coordinates, and averaged in 10° lat bands. Results are shown for statistics during (top) DJF and (bottom) JJA, with summer and winter hemispheres noted. Contour interval is 0.5×10^{-4} s^{-2}, with values above 4.5 shaded.

(independent of local vorticity), for DJF and JJA statistics (the summer statistics in Fig. 6 begin at 30° because there are relatively few $Z_{\mathrm{LRT1}} < 14$ km over 20°–30°). A clear maximum in N^2 is identified above the tropopause throughout the globe in Fig. 6, with maximum values 1–2 km above the tropopause. Over polar regions, the maximum in N^2 above the tropopause is substantially stronger in the summer hemisphere. However, the temperature anomaly associated with the TIL over the summer poles is difficult to separate from the background temperature increase with height. Over the winter poles a TIL is only weakly evident in N^2 (Fig. 6) or temperature.

The N^2 structure over midlatitudes in Fig. 6 shows relatively little difference between local summer and winter statistics, beyond the difference in latitudinal gradients (the winter statistics show larger N^2 maxima in low latitudes, whereas summer statistics show larger high-latitude N^2 maxima, as noted above). This similar behavior of the TIL between summer and winter is interesting, especially given the large seasonal variation in the height of the extratropical tropopause (e.g., Hoinka 1998; Birner 2006; Seidel and Randel 2006). The thickness of the maximum N^2 region shows a systematic increase from low to middle latitudes. This may be influenced by the presence of a lower stability region above the tropopause in the subtropics, which in turn is related to the proximity of the tropical tropopause [and the frequent occurrence of a secondary tropopause above Z_{LRT1}, as discussed in Randel et al. (2007)].

We have examined the longitudinal structure of the TIL, based on time-averaged statistics organized in latitude–longitude bins (in tropopause coordinates). This was motivated by the suggestion that the TIL might result from large-scale eddy heat fluxes (Birner 2006), in which case the strength of the TIL should reflect longitudinal structure in eddy fluxes (i.e., storm tracks). The strength of the inversion (quantified as in Fig. 5) shows relatively weak zonal structure for winter midlatitude statistics (maximum values vary from ~3.5 to 5 K), and almost no longitudinal variation in equinox or summer observations. The NH winter maximum occurs as a zonal wave 1 pattern, with maximum slightly east of the date line (somewhat downstream of the Pacific winter storm track); there is not a corresponding maximum over the Atlantic storm track. For SH winter a weak wave 1 is also evident, with maximum near the date line (somewhat downstream of the strongest winds, but distant from the eddy storm track maximum in the southern Indian ocean; Trenberth 1991). Overall the GPS data suggest that the strength of the TIL does not vary strongly in longitude, nor is it closely linked to storm track statistics.

4. A radiative forcing mechanism for the TIL

The global GPS observations demonstrate that the TIL is a ubiquitous feature of the extratropical tropopause. While the strength of the TIL is modulated by local dynamical structure (Figs. 4 and 5), the fact that it is evident for all circulation types suggests some additional forcing mechanism beyond baroclinic wave dynamics. Here we investigate a possible radiative mechanism for forcing and maintenance of the inversion layer.

At a given latitude the stratospheric temperature structure with height is influenced by the radiative effects of trace gases. In rough order of importance in the

lower stratosphere, these include ozone, water vapor, carbon dioxide, and other greenhouse gases [methane, nitrous oxide, and the chlorofluorocarbons (CFCs); e.g., Forster and Joshi 2005]. Ozone is particularly important as it absorbs significant amounts of solar radiation warming the stratosphere. It also warms the lower stratosphere in the longwave: as its absorption bands are relatively transparent and there is little ozone in the troposphere, irradiance emitted at a higher effective temperature close to the ground passes through the troposphere and is absorbed by ozone at a smaller effective temperature in the lower stratosphere. Water vapor in contrast causes the tropopause region and stratosphere to cool in the longwave, because of the small optical depth above the tropopause (see, e.g., Forster and Shine 2002).

To study the radiative effects of ozone and water vapor in this region, and include realistic vertical gradients, we calculate climatological profiles based in tropopause coordinates. We use winter (October–April) ozone and water vapor profiles from Boulder, Colorado, averaged with respect to the Z_{LRT1} (based on temperature profiles for each sounding). The results are shown in Fig. 7, together with the average temperature profile (also in tropopause coordinates), which shows a clear inversion layer. Ozone shows a strong increase above the tropopause, and there is evidence of a local peak in mixing ratio near the +2-km inversion level. Likewise the water vapor mixing ratios go from high values below the tropopause to its minimum stratospheric concentrations also around +1–2 km. Overall the ozone and water vapor profiles show that the transition region from tropospheric to stratospheric values occurs over altitudes ±1–2 km with respect to the thermal tropopause, and this is consistent with statistics derived from aircraft measurements near the tropopause (Pan et al. 2004).

The Reading narrowband radiative transfer model has been extensively used for stratospheric heating rate and temperature change calculations (e.g., Forster and Shine 2002), and we use it to investigate the radiative response near the tropopause to trace gas and cloud changes. The calculations here are based on a fixed dynamical heating assumption, wherein the dynamical contribution to heating is assumed to be the same in the background and perturbation calculations. Sensitivity tests were performed to examine the radiative temperature response to perturbations of trace gases, cloud, and aerosol, for a 42°N zonally averaged climatology. This climatology was created by merging the ozone and water vapor data in tropopause coordinates described above (5 km below to 5 km above the tropopause), with profiles from the standard Reading climatology.

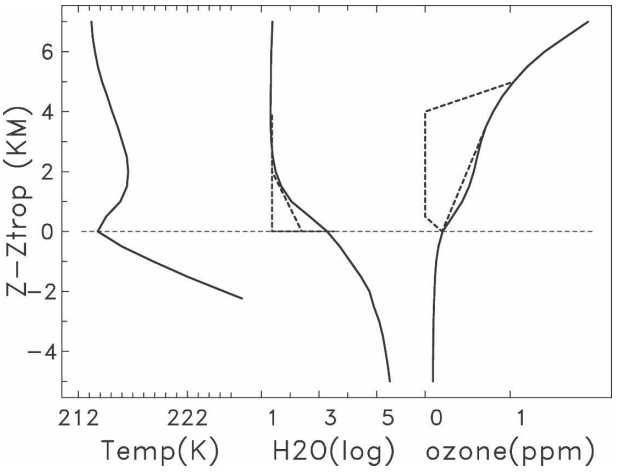

FIG. 7. Solid lines show vertical profiles of temperature, water vapor, and ozone in tropopause-based coordinates, derived from balloon measurements at Boulder, CO (40°N). Data are from the months October–April, spanning the years 1980–2004. Dashed lines in the water vapor and ozone profiles show the perturbations applied near the tropopause to test radiative heating effects.

Sensitivity tests with the radiative transfer model show that well-mixed greenhouse gases (CO_2, CH_4, N_2O, and the CFCs) do not affect heating rates or vary with altitude enough to significantly impact the vertical temperature gradients in the lowermost stratosphere. Similar tests perturbed high level cloud and stratospheric aerosol concentrations, but found that these were unable to account for the inversion. However, perturbations to the ozone and water vapor profiles revealed that ozone and water vapor have an important radiative influence near the tropopause. To estimate the contribution of ozone heating above the tropopause, we compare calculations where ozone is reduced or entirely removed for the region 0–4 km above the tropopause (as indicated in Fig. 7). The resulting temperature differences are shown in Fig. 8, showing that removing all of the ozone results in cooling of approximately 5 K, with a maximum near 2 km (in other words, the observed ozone contributes this magnitude of warming above the tropopause). Further analyses revealed that these ozone-associated temperature changes in the lower stratosphere were largely a longwave response (65% longwave; 35% shortwave). For water vapor, we compare the observed profile to two cases where the mixing ratio drops more rapidly to stratospheric levels above the tropopause (Fig. 7); that is, this tests the influence of water vapor over ~0–2 km. The resulting temperature differences (Fig. 8) show that the observed water vapor structure over 0–2 km contributes substantial cooling in this region (of order 5 K); this contributes to the coldness of the tropopause

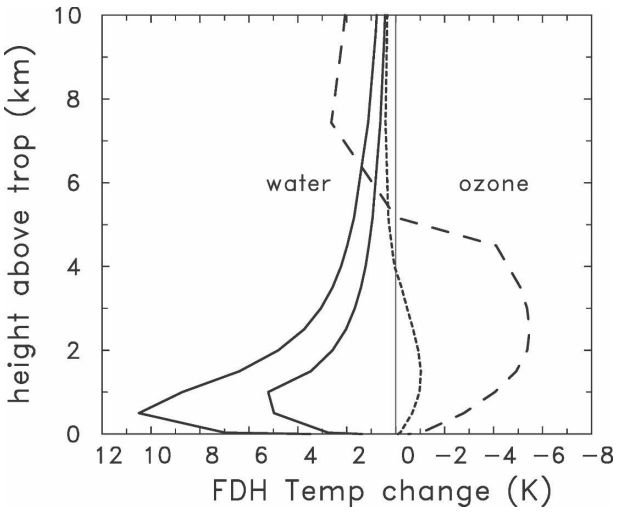

FIG. 8. Radiative sensitivity tests of lower-stratospheric temperature to ozone and water vapor perturbations near the tropopause (dashed lines in Fig. 7), based on fixed dynamical heating (FDH) calculations. The quantity shown is the temperature change resulting from the imposed changes; the abscissa is reversed to highlight the influence of the background ozone (warming) and water vapor (cooling) near the tropopause.

temperature minimum, and effectively enhances the strength of the inversion near 2–3 km. These results suggest that both ozone and water vapor play comparable roles in creating the inversion; the radiative effects are opposing but at slightly different altitude levels, which results in differential heating/cooling as a function of altitude.

5. Summary and discussion

High vertical resolution temperature profiles derived from GPS measurements show that the tropopause inversion layer is a ubiquitous feature of the extratropical tropopause. The TIL occurs in both hemispheres during all seasons, with an average magnitude of 3–5 K. The strength of the TIL is modulated by the local circulation, with a stronger inversion for anticyclonic flow (Figs. 4 and 5), as expected from balanced dynamics (Wirth 2003). However, the fact that the inversion is present for all circulation types suggests some additional forcing beyond balanced dynamics. The GPS data show that there are relatively small seasonal changes in the strength or structure of the TIL over middle latitudes (30°–60° N and S). In contrast, there is a large seasonal cycle in TIL magnitude over polar latitudes (60°–90° N and S), with a stronger inversion during summer. This seasonal variation at polar latitudes may be partly associated with the broad-scale background temperature structure above the tropopause, which increases with height in summer but not in winter. Note that the weaker TIL in winter high latitudes argues against a forcing mechanism primarily associated with baroclinic waves, as midlatitude eddies are substantially stronger (in the NH) during winter.

We suggest here that the radiative effects of ozone and water vapor near the tropopause may contribute a substantial component to forcing and maintenance of the TIL. Ozone acts to warm the region directly above the tropopause, while water vapor acts to cool the tropopause (and hence enhance the inversion). The strong vertical gradients of both constituents across the tropopause, and the details of the transition region, play a key role in the radiative balance. The chemical transition across the tropopause occurs within a layer several kilometers thick centered near the thermal tropopause (the so-called mixing layer, most clearly seen using tracer–tracer correlations; Hoor et al. 2002; Pan et al. 2004). This results in enhanced vertical gradients in ozone (and radiative heating) ~2–3 km above the tropopause, and also water vapor mixing ratios near the tropopause that are substantially higher than stratospheric values (with resulting radiative cooling of the tropopause). Hence the vertical scale of the inversion (maximum temperatures 2–3 km above the tropopause) may be partly linked to the thickness of the chemical transition layer. Although the processes controlling the thickness of the mixing layer are not well understood, the stability structure near the tropopause could be important, so that the chemical and thermal structure may be coupled in both directions. This radiative forcing mechanism can help explain the pervasive occurrence of the TIL, as strong vertical gradients in ozone and water vapor are a fundamental aspect of the extratropical tropopause. Furthermore, the fact that ozone heating contributes to the inversion layer (the shortwave component in particular) is consistent with the relatively weaker inversion observed over winter polar regions, and stronger inversion over the summer poles (as observed in Fig. 6). While the overall structure of the extratropical tropopause is tightly coupled to baroclinic wave dynamics (e.g., Haynes et al. 2001; Schneider 2004), our work suggests that radiative heating may play an important and perhaps dominant role for governing near tropopause temperature structure (despite relatively long radiative relaxation times in this region).

Acknowledgments. We thank several colleagues for discussions during the course of this work and comments on the manuscript, including Thomas Birner, Chris Davis, John Nielsen-Gammon, Rolando Garcia, Stephen Leroy, Dan Marsh, and Laura Pan. Construc-

tive reviews and suggestions by Volkmar Wirth and an anonymous reviewer helped improve the manuscript. The GPS temperature retrievals were processed by the University Corporation for Atmospheric Research (UCAR). The Boulder ozone and water vapor data were obtained from the Global Monitoring Division of the NOAA/Earth System Research Laboratory (http://www.cmdl.noaa.gov/ozwv/). This work was partially supported by the NASA ACMAP Program.

REFERENCES

Andrews, D. G., J. R. Holton, and C. B. Leovy, 1987: *Middle Atmosphere Dynamics.* Academic Press, 489 pp.

Birner, T., 2006: Fine-scale structure of the extratropical tropopause region. *J. Geophys. Res.,* **111,** D04104, doi:10.1029/2005JD006301.

——, A. Dörnbrack, and U. Schumann, 2002: How sharp is the tropopause at midlatitudes? *Geophys. Res. Lett.,* **29,** 1700, doi:10.1029/2002GL015142.

Forster, P. M., and K. P. Shine, 2002: Assessing the climate impact of trends in stratospheric water vapor. *Geophys. Res. Lett.,* **29,** 1086, doi:10.1029/2001GL013909.

——, and M. Joshi, 2005: The role of halocarbons in the climate change of the troposphere and stratosphere. *Climatic Change,* **71,** 249–266.

Hajj, G. A., and Coauthors, 2004: CHAMP and SAC-C atmospheric occultation results and intercomparisons. *J. Geophys. Res.,* **109,** D06109, doi:10.1029/2003JD003909.

Haynes, P. H., J. Scinocca, and M. Greenslade, 2001: Formation and maintenance of the extratropical tropopause by baroclinic eddies. *Geophys. Res. Lett.,* **28,** 4179–4182.

Hoinka, K. P., 1998: Statistics of the global tropopause pressure. *Mon. Wea. Rev.,* **126,** 3303–3325.

Hoor, P., H. Fischer, L. Lange, J. Lelieveld, and D. Brunner, 2002: Seasonal variations of a mixing layer in the lowermost stratosphere as identified by the CO-O_3 correlation from in situ measurements. *J. Geophys. Res.,* **107,** 4044, doi:10.1029/2000JD000289.

Hoskins, B. J., M. E. McIntyre, and A. W. Robertson, 1985: On the use and significance of isentropic potential vorticity maps. *Quart. J. Roy. Meteor. Soc.,* **111,** 877–946.

Kalnay, E., and Coauthors, 1996: The NCEP/NCAR 40-Year Reanalysis Project. *Bull. Amer. Meteor. Soc.,* **77,** 437–471.

Kursinski, E. R., and Coauthors, 1996: Initial results of radio occultation observations of earth's atmosphere using the Global Positioning System. *Science,* **271,** 1107–1110.

Pan, L. L., W. J. Randel, B. L. Gary, M. J. Mahoney, and E. J. Hintsa, 2004: Definitions and sharpness of the extratropical tropopause: A trace gas perspective. *J. Geophys. Res.,* **109,** D23103, doi:10.1029/2004JD004982.

Randel, W. J., D. J. Seidel, and L. L. Pan, 2007: Observational characteristics of double tropopauses. *J. Geophys. Res.,* **112,** D07309, doi:10.1029/2006JD007904.

Rocken, C., and Coauthors, 1997: Analysis and validation of GPS/MET data in the neutral atmosphere. *J. Geophys. Res.,* **102,** 29 849–29 866.

Schneider, T., 2004: The tropopause and the thermal stratification in the extratropics of a dry atmosphere. *J. Atmos. Sci.,* **61,** 1317–1340.

Seidel, D. J., and W. J. Randel, 2006: Variability and trends in the global tropopause estimated from radiosonde data. *J. Geophys. Res.,* **111,** D21101, doi:10.1029/2006JD007363.

Trenberth, K. E., 1991: Storm tracks in the Southern Hemisphere. *J. Atmos. Sci.,* **48,** 2159–2178.

Wickert, J., and Coauthors, 2001: Atmosphere sounding by GPS radio occultation: First results from CHAMP. *Geophys. Res. Lett.,* **28,** 3263–3266.

Wirth, V., 2000: Thermal versus dynamical tropopause in upper-tropospheric balanced flow anomalies. *Quart. J. Roy. Meteor. Soc.,* **126,** 299–317.

——, 2001: Cyclone–anticyclone asymmetry concerning the height of the thermal and the dynamical tropopause. *J. Atmos. Sci.,* **58,** 26–37.

——, 2003: Static stability in the extratropical tropopause region. *J. Atmos. Sci.,* **60,** 1395–1409.

——, 2004: A dynamical mechanism for tropopause sharpening. *Meteor. Z.,* **13,** 477–484.

——, and T. Szabo, 2007: Sharpness of the extratropical tropopause in baroclinic life cycle experiments. *Geophys. Res. Lett.,* **34,** L02809, doi:10.1029/2006GL028369.

Zangl, G., and V. Wirth, 2002: Synoptic-scale variability of the polar and subpolar tropopause: Data analysis and idealized PV inversions. *Quart. J. Roy. Meteor. Soc.,* **128,** 2301–2315.